Catal Lett (2009) 129:478–485
DOI 10.1007/s10562-008-9826-5

A Non-sodium Synthesis of Highly Ordered V-MCM-41 and Its Catalytic Application in Isomerization

Shuangquan Hu · Dapeng Liu · Lusi Li · Armando Borgna · Yanhui Yang

Received: 1 November 2008 / Accepted: 14 December 2008 / Published online: 9 January 2009

Abstract A rapid non-sodium process was developed to synthesize highly ordered V-MCM-41 mesoporous materials with atomic level dispersed vanadium species. $NH_3{\cdot}H_2O$ instead of NaOH was used to maintain the moderately basic synthesis condition. The characterization results of N_2 physisorption and XRD showed that the synthesized samples had highly ordered hexagonal structure. UV–Vis, UV-Raman, and EPR spectra provided evidence that most vanadium ions were tetrahedrally incorporated into the framework of siliceous MCM-41. The NH_3-TPD proved the mild acidity of V-MCM-41 due to the incorporation of vanadium cations. The most important variables were structural order and vanadium loading which can be controlled easily by changing synthesis variables in such a way that collapse of the V-MCM-41structure did not occur. The synthesized V-MCM-41 catalysts successfully catalyzed the isomerization of heptene. High conversion and isomer selectivity were achieved with good catalytic stability. The structure of V-MCM-41 can be well preserved after reaction.

Keywords V-MCM-41 · Non-sodium · Isomerization

Electronic supplementary material The online version of this article (doi:10.1007/s10562-008-9826-5) contains supplementary material, which is available to authorized users.

S. Hu · D. Liu · L. Li · Y. Yang (✉)
School of Chemical and Biomedical Engineering,
Nanyang Technological University,
Singapore 637459, Singapore
e-mail: yhyang@ntu.edu.sg

A. Borgna
Institute of Chemical Engineering and Sciences,
1 Pesek Road, Jurong Island 627833, Singapore

1 Introduction

MCM-41 has become one of the most popular mesoporous molecular sieves in the family of M41S, which was disclosed in 1992 by Mobil oil Corporation [1, 2]. Due to its unique properties, e.g., well defined mesostructure, narrow pore size distribution, tuneable pore diameter and high specific surface areas, MCM-41 has been widely used in heterogeneous catalysis, separation, electronics as well as optical fields [3, 4]. However, MCM-41 in its pure siliceous form shows limited applications in catalytic organic transformation due to the lack of active sites [3, 4]. Hence, modification is necessary by incorporating active components into the MCM-41 framework.

In recent years, the development of transition metal incorporated MCM-41 materials has attracted much attention in the fields of heterogeneous catalysis [5–7]. Exploring the novel formulation to produce metal incorporated mesoporous MCM-41 with a scalable process is the first critical step to achieve their industrialized application of these materials. Various preparation routes can be adopted to synthesize metal incorporated MCM-41 catalytic materials, e.g., ion-exchange [8, 9], post grafting [10], direct synthesis, impregnation [9–13], and chemical vapour deposition [14]. Most of these reported methods usually utilize NaOH to get an alkali solution or use Na_2SiO_3 as the silica source. However, the elimination of complications arising from sodium is highly desired for the application of metal ion incorporated MCM-41 as catalytic material because sodium has a negative effect in the substitution of metal ions, catalytic reactions, and stability [15]. Furthermore, the procedures of ion-exchange and post grafting methods are very complicated.

Vanadium containing MCM-41 has been widely investigated for the oxidation catalytic reaction [6, 16]. In this

study, rapid synthesis of vanadium incorporated MCM-41 (V-MCM-41) materials with well-ordered mesostructure in the absence of sodium is reported; the direct hydrothermal synthesis is formulated with the addition of ammonia solution. The effects of ammonia addition and vanadium incorporation will be discussed in detail.

Alkene isomerization has been receiving considerable attention in recent years, focusing mainly on butene isomerization [17, 18], as well as C5 and C6 alkene reactions [19–21]. The long chain naphtha is the main components of high octane gasoline. C7 alkenes represent one of the largest contributions to the alkene pool. Isomerization of C7 alkenes can increase the octane number of heavy naphtha dramatically, which has great potential for improving the resistance of a fuel to knock. Goddard et al. [22] studied the C7 alkene hydrotreating activity over $CoMo/Al_2O_3$, while Wehrer et al. [23] carried out C7 isomerisation of alkenes on molybdenum oxides under rapid flow of hydrogen. The iron-catalyzed alkene isomerization was also investigated [24]. However, the low surface areas of these catalysts have restricted their performances. As reported, MCM-41 shows much lower activity in catalytic cracking compared to USY or Beta zeolites because MCM-41 materials only presents mild acid sites [25, 26]. The incorporation of vanadium species manipulates the acidity on the MCM-41 pore wall surface to some extent. Along this line, one can predict that V-MCM-41 can be a good candidate for alkene isomerization. Herein, it is also reported the study of heptene isomerisation under hydrogen flow over V-MCM-41 mesoporous molecular sieves.

2 Experimental

2.1 Synthesis of V-MCM-41

In a typical synthesis of Si-MCM-41, 0.97 g of hexadecyltrimethyl-ammonium bromide (CTABr, >99%, Sigma) was dissolved in a certain amount of ammonia solution ($NH_3 \cdot H_2O$, 25%, VWR International) and distilled water. The total volume of ammonia solution and distilled water was maintained at 35 ml. The mixture was stirred till a clear solution was obtained. 4.5 g of tetraethyl orthosilicate (TEOS, 98%, Acros Organics) was added dropwise followed by adding a certain amount of 2% $VOSO_4$ ($VOSO_4 \cdot 3H_2O$, 99.99%, Aldrich) solution. After additional mixing for about 120 min, the synthesis gel was transferred into a PTFE lined autoclave placed in an oven at 120 °C for 48 h. After cooling to room temperature, the resulting solid was recovered by filtration, washed with deionized water and dried under ambient conditions. The pre-dried solid was heated at a constant rate from room temperature to 813.2 K over 20 h under He and held for 1 h under the same condition, followed by calcination at 813.2 K for 5 h with air to remove the residual surfactant. As the preparation process may cause some loss of vanadium and silica in the by-products, the final V content was determined by ICP analysis. The molar ratio composition of the gel mixture was 1TEOS: 0.12CTAB: $x NH_3 \cdot H_2O$: yV: $84.4H_2O$ where x varies from 9.2 to 18.5 (pH value from 12.5 to 14) and y varies from 0.012 to 0.035. The corresponding ammonia volume is 15–25 ml and the vanadium content is 1–3 wt%.

2.2 Characterization

Powder X-ray diffraction (XRD) patterns were recorded with a Bruker Advance 8 X-ray diffractometer equipped with a rotating anode using Cu Kα radiation ($\lambda = 0.154$ nm), operating at 40 kV and 40 mA. N_2 adsorption isotherms were measured at 77 K in a static volumetric Autosorb 6 (Quanta Chrome). Prior to measurements, samples were outgassed at 473 K to a residual pressure below 10^{-4} Torr. The specific surface area was calculated by the standard Brunauer–Emmett–Teller method (BET). The content of vanadium was determined by ICP analysis.

Diffuse reflectance UV–vis spectra were recorded on a VARIAN 5000 UV–VIS-NIR spectrophotometer in the range of 200–800 nm with pure Si-MCM-41 as reference. All samples were dried at 373 K overnight before performing the test. UV-Raman spectra were recorded using an excitation wavelength of 325 nm on a RENISHAW INVIA Raman microscope. Samples were pre-dried at 423 K overnight to remove the surface moisture. Electron paramagnetic resonance (EPR) measurements were carried out with Bruker EMX spectrometer at X-band ($\sim$9 GHz) under ambient conditions.

The temperature-programmed desorption (TPD) of ammonia was used to measure the acidic properties of the V-MCM-41 materials. The sample was activated at 773 K for 1 h under flowing helium and then cooled to 400 K before introducing anhydrous ammonia (5% in helium) for 30 min. Subsequently the physisorbed ammonia was removed by flushing with helium during 2 h at 400 K. The thermal desorption was conducted in flowing helium from 400 to 873 K using a heating rate of 8 K/min. Ammonia desorption was monitored continuously with a thermal conductivity detector. The outlet gas was passed through a 0.01 M H_2SO_4 solution to absorb the released NH_3. After adsorption, the solution was back-titrated to obtain total amount of desorbed ammonia.

2.3 Heptene Isomerization

Typically, 200 mg catalyst was loaded in the quartz reactor which was equipped with the thermocouple beside the

catalyst bed for better monitoring of the pre-treatment and reaction temperature. The reactor was installed vertically inside a 35 mm i.d. tubular furnace controlled by a programmable PID temperature controller. Before each reaction run, the catalyst was pre-treated in situ in a hydrogen stream at 673 K for 1 h. Hydrogen was regulated by mass flow controller at 20 ml/min. Heptene with constant flow rate of 0.005 ml/min was controlled by a HPLC pump. The volume ratio of reactant feed mixture is 4.2 vol% heptene vapour and 95.8 vol% hydrogen. The weight hourly space velocity (WHSV) was changed from 0.5 to 2 h^{-1} by changing the catalyst weight. The entire microreactor, including the pipelines, was heated at 393 K to vaporize the heptene and avoid condensation of the products. The feedstock and products were analyzed by an online gas chromatograph (Agilent 6890) equipped with FID detector and PONA column.

3 Results and Discussion

3.1 X-ray Diffraction

It is well known that MCM-41 is typically characterized by an X-ray reflection in the vicinity of $2\theta = 2$ °. In MCM-41 samples, the XRD peaks do not result from local order in the atomic range, but from the ordered channel walls. The powder XRD patterns of the calcined Si-MCM-41 and V-MCM-41 samples are shown in Fig. 1. Figure 1a shows the XRD patterns of Si-MCM-41 prepared with different amounts of ammonia. A well ordered two-dimensional hexagonal structure can be observed, giving a sharp (100) plane diffraction peak and the diffraction peaks of higher miller index planes, (110), (200), (210), and (300). The Si-MCM-41 sample prepared with modest amount of ammonia shows the best structure, suggesting that the alkali environment will affect the hydrothermal synthesis to some extent, which is in good agreement with the literature reported elsewhere [27]. The vanadium incorporated MCM-41 samples (V-MCM-41) exhibit similar structure to that of Si-MCM-41 (Fig. 1b). The main (100) diffraction peaks of V-MCM-41 samples shift to lower angle compared to that of Si-MCM-41, which may be caused by (1) the incorporation of vanadium ions in which V–O has longer bond than that of the Si–O, and (2) the thickening of the pore wall due to the transition-metal-promoted cross-linking of the amorphous silica walls [28].

3.2 Nitrogen Physisorption

The nitrogen physisorption was conducted for a series of V-MCM-41 samples with different vanadium contents. The nitrogen adsorption/desorption isotherms and the corresponding pore size distributions are depicted in Fig. 2. The isotherms are assigned to type Langmuir IV isotherm according to the IUPAC classification. The capillary condensation shows a sharp step increase in the relative pressure (P/Po) range of 0.3–0.4 for all V-MCM-41 samples, suggesting typical mesoporous structure with uniform pore diameters. The uniformity of the pore structure changes with the incorporation of vanadium cations. The more the vanadium incorporation, the broader the pore size distribution of V-MCM-41 samples (Fig. 2b). Apparently, the incorporation of a large amount of vanadium disrupts the structure of V-MCM-41 over some distance, which is similar to the effect of other transition metal ions on the MCM-41 structure reported elsewhere [29]. The physicochemical properties of

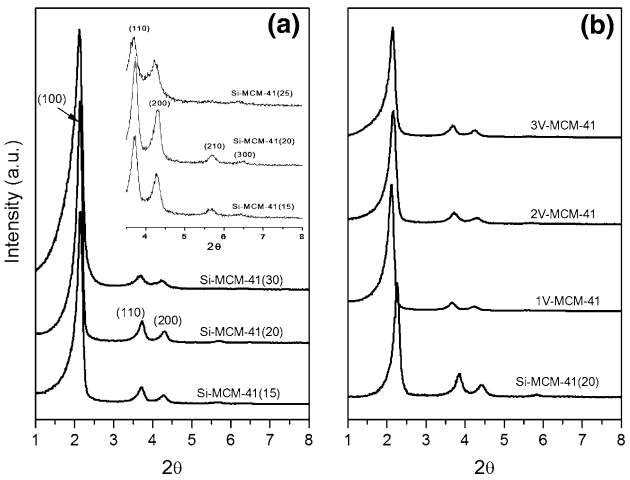

Fig. 1 X-ray diffraction patterns of Si-MCM-41 and V-MCM-41: **a** Si-MCM-41 synthesized with different amounts of ammonia; **b** V-MCM-41 with different vanadium content

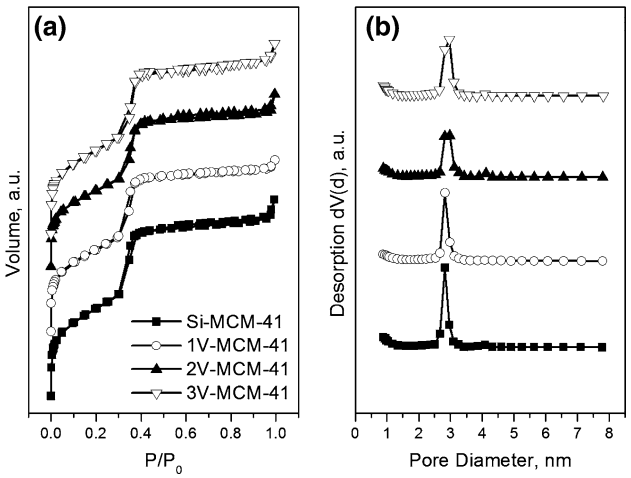

Fig. 2 Nitrogen physisorption of V-MCM-41 with different vanadium loading **a** isotherm graph of Si-MCM-41, 1 V-MCM-41, 2 V-MCM-41 and 3 V-MCM-41 **b** Pore size distribution of Si-MCM-41, 1 V-MCM-41, 2 V-MCM-41 and 3 V-MCM-41

Table 1 List of physicochemical properties of Si-MCM-41 and V-MCM-41

V content[a] (wt %)	Test V content[b] (wt %)	BET surface area (m^2/g)	Mesopore volume (cc/g)	Pore volume (cc/g)	Pore diameter (nm)	*d*-spacing (nm)	Wall thickness (nm)
0	0	970	0.98	1.10	2.83	3.93	1.71
1	0.59	877	0.93	1.00	2.82	4.20	2.04
2	0.93	810	0.85	0.95	2.97	4.10	1.77
3	1.42	922	0.95	1.79	2.97	4.14	1.81

[a] Vanadium content added when synthesis

[b] Vanadium content tested by ICP

V-MCM-41 samples are summarized in Table 1. The surface area and pore volume decrease when large amount of vanadium is incorporated. The pore diameter and wall thickness become larger as the result of the vanadium incorporation into the MCM-41 silica framework.

3.3 Diffuse Reflectance UV–Vis Spectroscopy

The local environmental formation of metal cations in an oxide domain can be revealed by UV–Vis spectroscopy. It is known that the quantum size effect results in the relationship between the optical band gap energy and the domain size. Diffuse reflectance UV–Vis spectra of V-MCM-41 samples are shown in Fig. 3a. There is no absorbance in the range of 600–800 nm region, indicating the lack of the characteristic *d–d* transitions of $(VO)^{2+}$ [30]. This is probably caused by the valence of vanadium changing from 4+ to 5+ during the calcination. All samples show absorbance bands in 247 and 374 nm, which are attributed to the isolated vanadium species incorporated into the framework and on the pore wall surface, respectively [11, 31]. The absence of the 320 and 450 nm bands indicates there is no polymeric V–O–V bond and V_2O_5 crystallites in these V-MCM-41 materials [11].

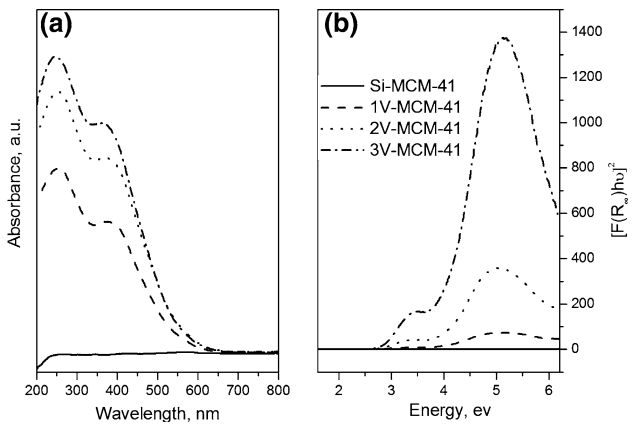

Fig. 3 UV–vis spectrum of V-MCM-41, **a** absorbance graph of V-MCM-41 **b** UV absorption edge of V-MCM-41

The shape and shift of the absorption edge of the UV–Vis spectrum are useful in understanding the basic mechanism of optically induced transitions in crystalline and non-crystalline materials, providing local structural coordination information. The edge position is determined in a classic approach [32] by finding the energy intercept of a straight line fitted through the low energy rise in the profile of $[F(R_\infty) \times h\nu]^2$ versus $h\nu$, where $F(R_\infty)$ is the Kubelka–Munk function. This suggests an expression to correlate the absorption coefficient to photon energy, and the order of the power function depends on whether the transitions are allowed or forbidden [33]. However, different order of power is determined simply by the best linear fit of the energy gap curve for the cases of vanadium oxide species. The V-MCM-41 and referential samples with standard compounds (V_2O_5, NH_4VO_3, PbV_2O_6, and Na_3VO_4) are tested. The transformations of $[F(R_\infty) \times h\nu]^2$ versus $h\nu$ of samples 1 V-MCM-41, 2 V-MCM-41 and 3 V-MCM-41 are shown in Fig. 3b. The absorption band reflects a ligand to metal charge transfer band (LCT) transition [6]. Band gap edge energies of various V-MCM-41 samples are shown in Table 2. All the band gap edge energies of

V-MCM-41 samples fall into the region between Na_3VO_4 (tetrahedral) and NH_4VO_3 (distorted tetrahedral) indicating

Table 2 List of edge position of V-MCM-41 samples and the standard samples

Sample name	Edge position (eV)	Standard sample[a]	Edge position (eV)	Coordination condition
Si-MCM-41	–	Na_3VO_4	4.4	Tetrahedral
1 V-MCM-41	4.16	NH_4VO_3	3.2	Distorted tetrahedral
2 V-MCM-41	3.98	PbV_2O_6	2.8	Distorted octahedral
3 V-MCM-41	4.04	V_2O_5	2.4	Square pyramidal

[a] The standard samples are prepared by mixed pure chemical with Si-MCM-41 by grinding

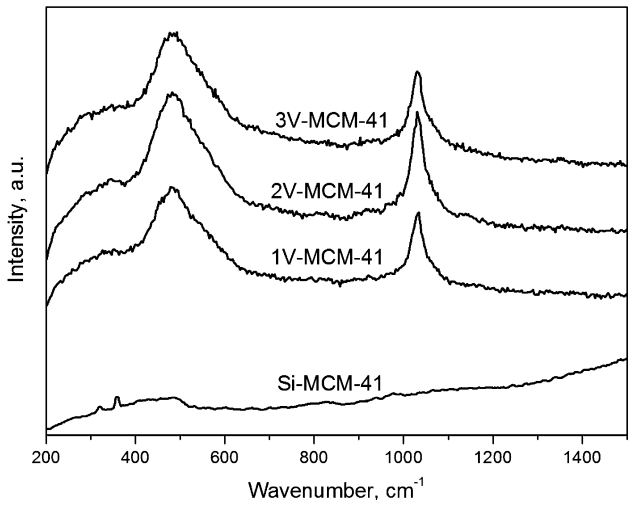

Fig. 4 Raman spectra V-MCM-41 materials

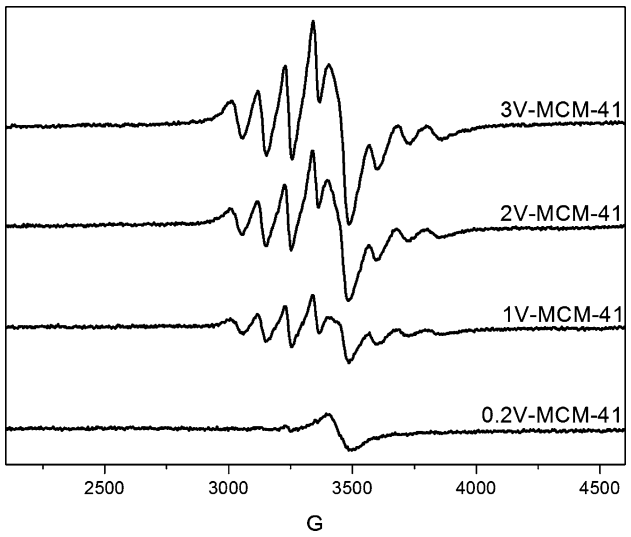

Fig. 5 EPR spectra (1st derivative) of 0.2 V-MCM-41, 1 V-MCM-41, 2 V-MCM-41, and 3 V-MCM-41

that the vanadium species in these V-MCM-41 samples is located in the distorted tetrahedral coordination.

3.4 UV-Raman Spectroscopy

UV-Raman spectroscopy is used to elucidate the molecular nature of vanadium domains. The Raman spectra of V-MCM-41 samples with different vanadium loading are shown in Fig. 4. The peak at 486 cm^{-1} is due to the three-fold siloxane rings and siloxane bridges on the silica support [34]. A strong Raman band at $\sim$1,033 cm^{-1} assignable to the symmetric V=O stretching vibration of isolated VO_4 species can be observed for all the V-MCM-41 samples [34–36]. The broad Raman band at $\sim$915 cm^{-1} is the characteristics of Si–O– and Si(–O–)$_2$ functionalities corresponding to the perturbation in silica vibrations, which may be an indication of the V–O–Si formation [37]. No significant band at $\sim$141 cm^{-1} corresponding to crystalline V_2O_5 can be observed. Furthermore, the absence of typical band at 995 cm^{-1} of V_2O_5 implies no polymeric crystalline V_2O_5 is formed in the V-MCM-41 samples, which is in good agreement with UV–Vis results. These observations suggest the vanadium domains in the siliceous framework or on the pore wall surface are all in an isolated state, without aggregation to form crystalline V_2O_5.

3.5 Electron Paramagnetic Resonance

Electron Paramagnetic Resonance is a powerful and sensitive technique for investigating the oxidation states, surfaces, bulk coordination and the physical form of a transition metal oxide. V^{4+} cations are very convenient EPR probes because the ^{51}V (natural abundance 99.8%) nuclei have a large magnetic moment leading to informative hyperfine structures (S = 1/2; I = 7/2). Figure 5 shows the EPR spectra of calcined V-MCM-41 samples. There is no tetravalent vanadium (V^{4+}) signal shown for 0.2 wt% V-MCM-41 sample, which indicates that nearly all vanadium has been oxidized to 5 + during the calcination. However, samples with higher V content show an axially symmetrical signal of tetravalent vanadium which originated from the d^1 electron interaction with nuclear spin signals with nuclear spin of ^{51}V. The spectrum indicates only one vanadium site and the spin Hamiltonian parameters are $g = 1.984$ and $A = 110G$ where A is the hyperfine coupling constant. This signal can be assigned to tetrahedrally coordinated vanadium inside the pore wall of MCM-41, which cannot be fully oxidized during the calcination. No spin–spin interaction among V^{4+} ions indicates that V^{4+} is highly dispersed in the silica framework [38, 39].

3.6 Ammonia Temperature Programmed Desorption (NH_3-TPD)

The temperature programmed desorption of basic molecule such as ammonia (NH_3-TPD) is one of the most commonly used methods for measuring the surface acidity of porous materials [44]. The NH_3-TPD profiles of 1 V-MCM-41, 2 V-MCM-41 and 3 V-MCM-41 samples are shown in Fig. 6. Only one broad desorption peak is observable at medium temperature range, and the peak position is almost identical at 524 K for all the samples, suggesting the similar acidity strength which is in the mild acidity range. The total amount of Bronsted acid sites increases with the content of vanadium incorporated in the silica framework of MCM-41. The calculated acidity amount for 1 V-MCM-41, 2 V-MCM-41 and 3 V-MCM-41 are 0.012, 0.048, and 0.097 mol/g, respectively. The correlation between total

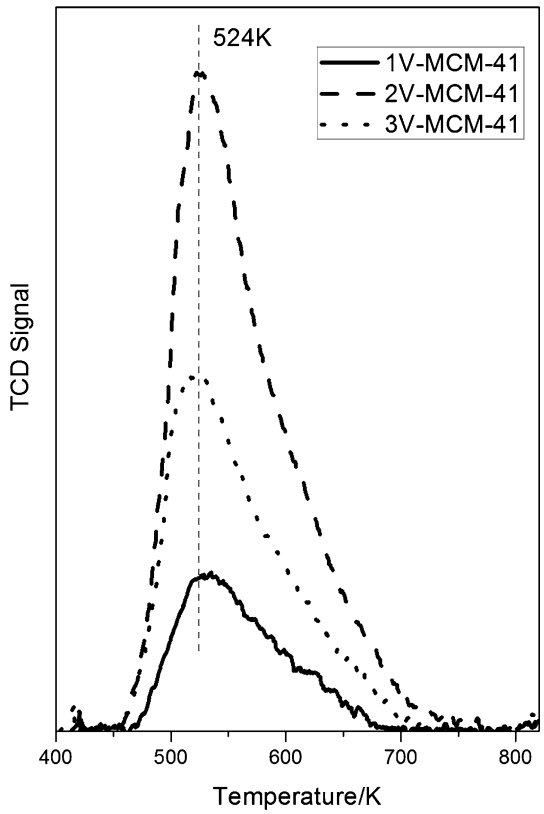

Fig. 6 NH_3-TPD results of V-MCM-41 materials

acidity amount and vanadium content gives the evidence that the acidity in the V-MCM-41 is mainly caused by the vanadium sites in the structure [41].

3.7 Heptene Isomerization

In this study, V-MCM-41 is demonstrated as a good catalyst to catalyze the heptene isomerization due to its mild acidity. Alkene isomerization shows more complicated reaction scheme compared to alkane isomerization. Besides the skeletal isomerization and double bond shift, hydrogenation of alkene to the corresponding alkane accompanies isomerization under hydrogen environment. In this study, the isomer selectivity is defined as the total isomerization (skeletal isomerization and double bond shift reaction) over the total C7 conversion (skeletal isomerization, double bond shift reaction, and hydrogenation).

The conversion and isomer selectivity of heptene isomerization over V-MCM-41 samples are shown in Fig. 7. Pure siliceous Si-MCM-41 exhibits the conversion of around 10% and does not change significantly with temperature. The low conversion is probably due to the weak acidic sites of Si-MCM-41 arouse from the silanol groups on the pore wall surface [42]. The isomer selectivity ($\sim$92%) stays constant within the range of reaction temperature tested in this study. For 1 V-MCM-41, 2 V-MCM-41, and

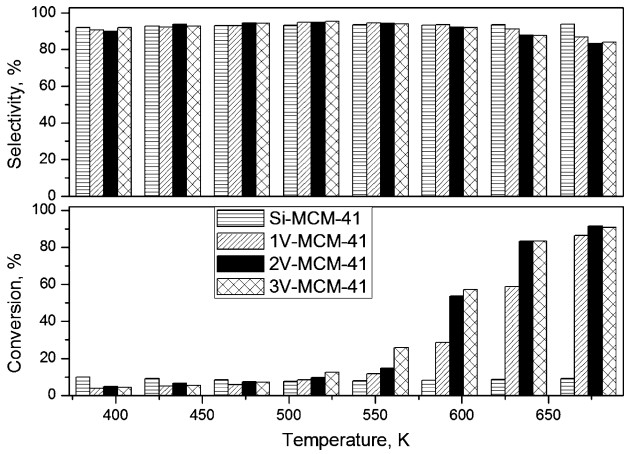

Fig. 7 Catalytic results about the conversion and selectivity of heptene isomers by Si-MCM-41, 1 V-MCM-41, 2 V-MCM-41 and 3 V-MCM-41

3 V-MCM-41 catalyst, the conversion of heptene is similar with the Si-MCM-41 when temperature is below 550 K, whereas a remarkable increase of heptene conversion occurs at the temperature above 550 K. The conversion reaches 90% at 673 K and the selectivity maintains above 83%, suggesting that vanadium cations bring stronger acidic sites into V-MCM-41 than that of silanol group and these acidic sites become more active at the temperature above 550 K [41]. Increasing vanadium content from 1 to 3 wt % gives higher conversion under high temperature (>650 K). The selectivity of isomers slightly decreases for the V-MCM-41 catalyst with high vanadium content, e.g., from 94 to 84% for 3 V-MCM-41 at temperature about 650 K due to more hydrogenation occurs at high temperature. These results indicate that V-MCM-41 may favor both isomerization and hydrogenation at high temperature, although isomers are still the main product. The absence of cracking and cycloalkene products, even under high temperature (650 K), suggests the good potential for industry application of V-MCM-41 as a catalyst for alkene isomerization.

Activation energy of the reaction was calculated using Arrhenius plot shown in Fig. 8. Two stage of linear relationship is observed. The activation energies for 1 V-MCM-41, 2 V-MCM-41 and 3 V-MCM-41 are calculated as 10.2, 10.3 and 10.2 kJ/mol, respectively between temperature of 513 and 393 K, which may be attributed to the diffusion limitation of heptene in the V-MCM-41 channels under low temperature. The activation energies are 52.4, 46.8, and 32.7 kJ/mol for 1 V-MCM-41, 2 V-MCM-41 and 3 V-MCM-41, respectively between temperature 550 and 700 K. The decrease of activation energy can be explained by the addition of more O-vacancy when vanadium cations incorporate into the silica framework [43, 44].

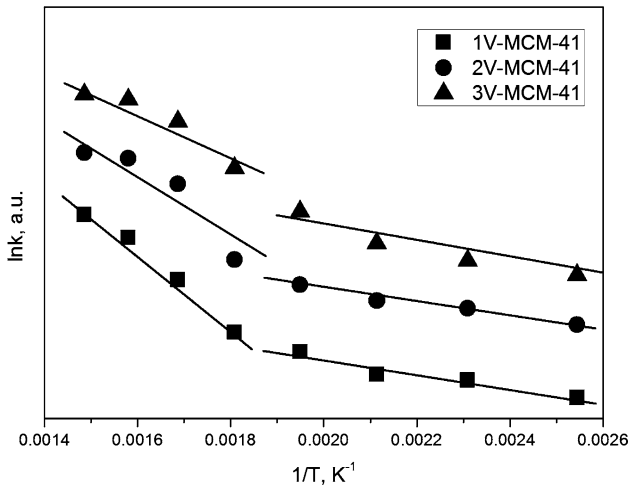

Fig. 8 Linear relationship between lnk vs 1/T for V-MCM-41

Weight hourly space velocity (WHSV) effect was tested by varying the weight of 2 V-MCM-41 catalyst, shown in Fig. 9 (WHSV $= 0.5, 1, 2\ h^{-1}$). Increasing WHSV leads to a lower heptene conversion due to the insufficient contact between catalyst and reactant flow. Interestingly, the selectivity of isomer was observed to increase with the space velocity at elevated temperature, suggesting that high WHSV is favorable to isomerization than hydrogenation. When the temperature is above 673 K, the effect of different WHSV on heptene conversion becomes less significant.

The long-term stability of 2 V-MCM-41 catalyst was tested under 593 K for 40 h as shown in Fig. 10. The conversion gradually decreases, whereas the selectivity of isomers shows a rapid increase via reaction time. After 1,600 min, the stabilized conversion and isomer selectivity are 70 and 93%, respectively. N_2 physisorption and XRD tests illustrate that this particular V-MCM-41 sample still preserves its good hexagonal structure after 40 h reaction (see supporting information).

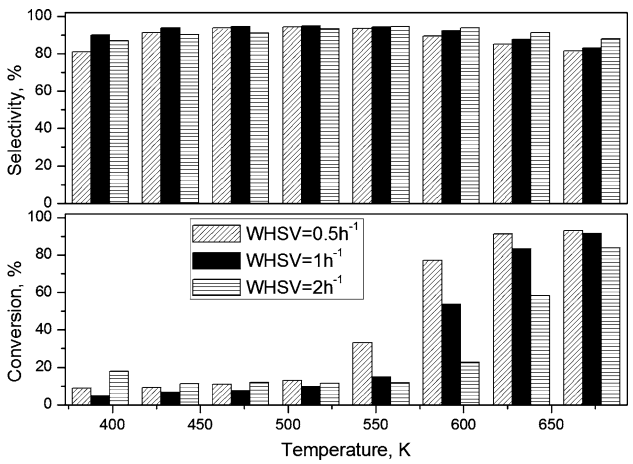

Fig. 9 Conversion and selectivity of isomers with different WHSV (0.5, 1, 2 h^{-1}) on 2 V-MCM-41

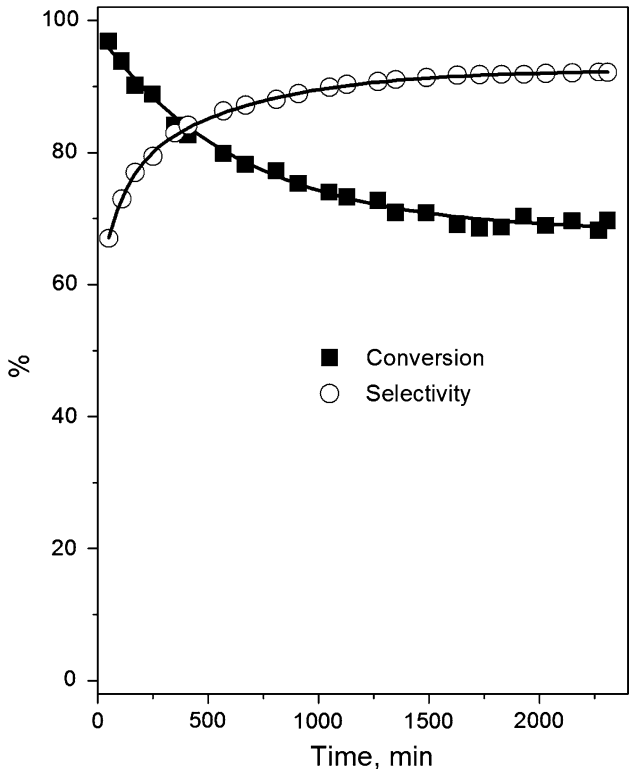

Fig. 10 Conversion and selectivity of isomers over long time test on 2 V-MCM-41 under 593 K

4 Conclusion

A series of highly ordered V-MCM-41 samples were successfully synthesized rapidly using ammonia solution. The XRD and N_2 adsorption/desorption showed that the samples possess highly ordered structure and narrow pore size distribution. UV–Vis, UV-Raman, and EPR characterizations indicated that the vanadium ions in the mesoporous molecular sieves were in a tetrahedral coordination and distributed on the pore wall surface with an atomic level dispersion. The heptene isomerization results showed that V-MCM-41 catalysts presented high conversion and isomer selectivity because of its mild acidity brought by the vanadium incorporation.

Acknowledgments The authors thank AcRF tier 2 (M45120006 ARC 13/07) for providing funding support. The financial support of AcRF tier 1 (M52120049 RG45/06) is gratefully acknowledged.

References

1. Beck JS, Vartuli JC, Roth WJ, Leonowicz ME, Kresge CT, Schmitt KD, Chu CTW, Olson DH, Sheppard EW, McCullen SB, Higgins JB, Schlenker JL (1992) J Am Chem Soc 114:10834–10843
2. Kresge CT, Leonowicz ME, Roth WJ, Vartuli JC, Beck JS (1992) Nature 359:710–712

3. Xu JQ, Chu W, Luo SZ (2006) J Mol Catal A-Chem 256:48–56
4. Ying JY, Mehnert CP, Wong MS (1999) Angew Chem Int ED 38:56–77
5. Dapurkar SE, Sakthivel A, Selvam P (2004) J Mol Catal A-Chem 223:241–250
6. Kwak JH, Herrera JE, Hu JZ, Wang Y, Peden CHF (2006) Appl Catal A-Gen 300:109–119
7. Chen Y, Ciuparu D, Lim S, Haller GL, Pfefferle LD (2006) Carbon 44:67–78
8. Gucbilmez Y, Dogu T, Balci S (2005) Catal Today 100:473–477
9. Zhang QH, Wang Y, Ohishi Y, Shishido T, Takehira K (2001) J Catal 202:308–318
10. Pena ML, Dejoz A, Fornes V, Rey E, Vazquez MI, Nieto JML (2001) Appl Catal A-Gen 209:155–164
11. Solsona B, Blasco T, Nieto JML, Pena ML, Rey F, Vidal-Moya A (2001) J Catal 203:443–452
12. Du GA, Lim SY, Yang YH, Wang C, Pfefferle L, Haller GL (2006) Appl Catal A-Gen 302:48–61
13. Parida KM, Rath D (2006) J Mol Catal A-Chem 258:381–387
14. Grubert G, Rathousky J, Schulz-Ekloff G, Wark M, Zukal A (1998) Micropor Mesopor Mat 22:225–236
15. Xia QH, Chen X, Tatsumi T (2001) J Mol Catal A-Chem 176: 179–193
16. Selvam P, Dapurkar SE (2005) J Catal 229:64–71
17. de Menorval B, Ayrault P, Gnep NS, Guisnet M (2005) J Catal 230:38–51
18. de Menorval B, Ayrault P, Gnep NS, Guisnet M (2006) Appl Catal A-Gen 1–13
19. Guo J, Cheng XW, Zhou WZ, Long YC (2005) Micropor Mesopor Mat 79:319–328
20. Tiitta M, Harlin E, Makkonen J, Root A, Sandelin F, Osterholm H, (2004) In: Recent advances in the science and technology of zeolites and related Materials, Pts a–c, pp 2323–2330
21. Li DD, Li MF, Chu Y, Nie H, Shi YH (2003) Catal Today 81:65–73
22. Goddard SA, Kukes SG (1994) Energ Fuel 8:147–150
23. Wehrer P, Libs S, Hilaire L (2003) Appl Catal A-Gen 238:69–84
24. Glascoe EA, Sawyer KR, Shanoski JE, Harris CB (2007) J Phys Chem C 111:8789–8795
25. Taguchi A, Schuth F (2005) Micropor Mesopor Mat 77:1–45
26. Auroux A (2002) Top Catal 19:205–213
27. Lim S, Ciuparu D, Yang YH, Du GA, Pfefferle LD, Haller GL (2007) Micropor Mesopor Mat 101:200–206
28. Parvulescu V, Anastasescu C, Constantin C, Su BL (2003) Catal Today 78:477–485
29. Shylesh S, Singh AP (2005) J Catal 233:359–371
30. Yang YH, Lim S, Du GA, Chen Y, Ciuparu D, Haller GL (2005) J Phys Chem B 109:13237–13246
31. Shylesh S, Singh AR (2006) J Catal 244:52–64
32. Yang YH, Du GA, Lim SY, Haller GL (2005) J Catal 234:318–327
33. Weber RS (1995) J Catal 151:470–474
34. Davis EA, Mott NF (1970) Philos Mag 22:903–922
35. Das N, Eckert H, Hu HC, Wachs IE, Walzer JF, Feher FJ (1993) J Phys Chem 97:8240–8243
36. Went GT, Oyama ST, Bell AT (1990) J Phys Chem 94:4240–4246
37. Ying F, Li JH, Huang CJ, Weng WZ, Wan HL (2007) Catal Lett 115:137–142
38. Chatterjee M, Iwasaki T, Hayashi H, Onodera Y, Ebina T, Nagase T (1999) Chem Mater 11:1368–1375
39. Subrahmanyam C, Louis B, Viswanathan B, Renken A, Varadarajan TK (2005) Appl Catal A-Gen 282:67–71
40. Rodriguez-Gonzalez L, Hermes F, Bertmer M, Rodriguez-Castellon E, Jimenez-Lopez A, Simon U (2007) Appl Catal A-Gen 328:174–182
41. Lim S, Haller GL, Phys J (2002) Chem B 106:8437–8448
42. Slomkiewicz PM (2006) Appl Catal A-Gen 301:232–240
43. Goodrow A, Bell AT, Phys J (1320) Chem C 112(34):4–13214